Hydrometallurgy 184 (2019) 162–174

Contents lists available at ScienceDirect

Hydrometallurgy

journal homepage: www.elsevier.com/locate/hydromet

Selective rare earth element extraction using high-pressure acid leaching of slags arising from the smelting of bauxite residue

Rodolfo Marin Rivera[a], Buhle Xakalashe[b], Ghania Ounoughene[a], Koen Binnemans[c], Bernd Friedrich[b], Tom Van Gerven[a,*]

[a] Department of Chemical Engineering, KU Leuven, Celestijnenlaan 200F, B-3001 Heverlee, Belgium
[b] Institute of Process Metallurgy and Metal Recycling, RWTH Aachen University, 52056 Aachen, Germany
[c] Department of Chemistry, KU Leuven, Celestijnenlaan 200F, B-3001 Heverlee, Belgium

ARTICLE INFO

Keywords:
High-pressure acid leaching
Bauxite residue
Rare earths
Red mud
Slag
Smelting

ABSTRACT

During acid leaching of bauxite residue (red mud), the increase in dissolution of rare-earth elements (REEs) is associated with a substantial co-dissolution of iron; this poses problems in the downstream processing (i.e. solvent extraction or ion exchange). Six different slags generated by reductive smelting of the same bauxite residue sample were treated by high-pressure acid leaching (HPAL) with HCl and H_2SO_4 to selectively extract REEs. Thus, up to 90 wt% of scandium was extracted from the slags using H_2SO_4 at 150 °C, while with HCl the extraction of scandium reached up to 80 wt% at 120 °C. The extraction of yttrium, lanthanum and neodymium was above 95 wt% when HCl was used as a reagent, but it was much lower (< 20 wt%) with H_2SO_4, presumably due to the formation of a double sulfate ($NaLn(SO_4)_2 \cdot nH_2O$) and/or due to the adsorption on the surface of silicon/aluminium-oxides compounds. In addition, HPAL of bauxite residue slags led to a significant co-dissolution of aluminium (> 90 wt%, 18 g L^{-1}), while the concentration of the remaining iron (> 60 wt%) was of 3 g L^{-1} in the leachate. The co-dissolution of silicon and titanium was lower than 5 wt%.

1. Introduction

Over 95% of the worldwide produced alumina is processed by the Bayer process (World Aluminium and the European Aluminium Association, 2015). The process consists in contacting aluminium-bearing ores with NaOH at temperatures between 150 and 250 °C, in autoclaves or tubular reactors, at pressures of up to about 4 MPa (Power et al., 2011). As the process is carried out at high pH values (about 14), aluminium hydroxides are selectively dissolved from bauxite minerals, while most of the other compounds remain insoluble in the bauxite residue. Annually, about 1.35 t of bauxite residue are generated per tonne of alumina produced (Deady et al., 2016; Evans, 2016). It is believed that the inventories of bauxite residue have increased up to 4 billion tonnes, with an annual growth rate of approximately 160 million tonnes (Klauber et al., 2011).

Bauxite residue is mainly composed of metallic oxides of aluminium, iron and titanium, but also of rare-earth elements (REEs) (Binnemans et al., 2015). Soda and silica are also present. The chemical composition is very wide, as it depends on the origin of the mineral ore and also on the operational conditions used during the production of purified aluminium hydroxide from bauxite minerals. A typical range of component in bauxite residue has already been reported elsewhere (Evans, 2016). Rare-earths are contained in minor extent, but their concentration can be as high as 1300 mg kg^{-1} (Ochsenkuhn-Petropulu et al., 1994). Scandium represents about 90% of the economic value of the REEs present in bauxite residue, and its concentration can be as high as 260 mg kg^{-1} (Borra et al., 2016a; Wagh and Pinnock, 1987). This concentration is higher than the average abundance in the Earth's crust (22 mg kg^{-1}), and significantly enriched compared to that in the original bauxite ore (Ochsenkühn-Petropulu et al., 1996).

Although conventional acid leaching with different mineral acids (e.g., HCl, H_2SO_4, HNO_3) can partially or fully extract REEs from bauxite residue, the leaching process is controlled by intra-particle diffusion as metals are transported from the solid phase to the solution through the cracks and pores present in the particles (Liu et al., 2009; Reid et al., 2017). However, the co-dissolution of silicon and iron represents a drawback in the downstream processing (e.g., solvent extraction or ion exchange). A high concentration of silicon in the leach solution can lead to silica gel formation, which significantly affects the leaching efficiency as the gel solution can no longer be filtered. It is believed that these aggregates may act as a resistance for the acid solution as they are partially adsorbed on the surface of bauxite residue

* Corresponding author.
E-mail address: tom.vangerven@kuleuven.be (T. Van Gerven).

https://doi.org/10.1016/j.hydromet.2019.01.005
Received 22 August 2018; Received in revised form 3 December 2018; Accepted 14 January 2019
Available online 17 January 2019
0304-386X/

minerals (Rivera et al., 2017b). Meanwhile, the co-dissolution of iron is detrimental as it is difficult to separate it from the rare-earths, particularly from scandium, requiring a large quantity of reagents during the downstream processing. Scandium(III) ions are present in the iron(III)-rich oxide lattice (Vind et al., 2018a; Zhang et al., 2017), which limits its complete dissolution (Borra et al., 2015; Rivera et al., 2017a). Therefore, iron must be removed in advance in order to improve the extraction and selectivity of REEs.

Smelting of bauxite residue leads to the reduction of iron oxides to produce pig iron, i.e. a metallic product generated from a smelting furnace with an iron content usually above 90 wt% (Alkan et al., 2017; Jayasankar et al., 2012), and a REE-rich slag (Borra et al., 2016b; Kaußen and Friedrich, 2015; Yagmurlu et al., 2017). The process strongly depends on flux consumption and/or high operating temperature due to the high concentration of alumina. The relatively large volume of fluxes may increase not only the energy consumption during smelting, but also the acid consumption during leaching. The removal of alumina by alkali roasting before the smelting process was proposed by Borra et al. to diminish the flux consumption (Borra et al., 2017; Kaußen and Friedrich, 2015). Although the method allows for the recovery of alumina as a valuable by-product, the roasting step must be carried out at temperatures of about 500 °C (when NaOH is used as a reducing agent), while the smelting stage is carried out at 1500 °C without using fluxes for iron removal. Although the energy consumption of the process is about 3.5 GJ tonne^{-1}, i.e. similar to the energy consumption reported by direct (reductive) smelting of bauxite residue (Borra et al., 2016c), the volume of slag generated by this process is about 50% lower than the volume of slag produced by the direct smelting process, which limits the amount of REEs that can be further recovered. Reductive smelting allows the separation of iron from the rare-earths which can be highly enriched, together with a significant amount of aluminium and silicon, in the slag phase. REEs can then be extracted by leaching the slag with mineral acids. The extraction efficiency of REEs from the slag during leaching, however, is determined by their mineralogical association during solidification of the slag after smelting. It has been reported that perovskite ($CaTiO_3$) phase, formed during solidification, has the capability of converting the lanthanides into titanate solid solutions, $Ca_xLn_{(1-x)}TiO_3$, which are very difficult to leach. However, their formation can be avoided by applying a rapid cooling rate (or rapid solidification) of the slag (Borra et al., 2017; Shrivastava et al., 2004). Nonetheless, little is known about the mineralogy and chemical speciation of REEs in slags arising from bauxite residue smelting. However, it is most likely that REE do not occur in the elemental state, nor do they occur as individual rare earth compounds due to their strong affinity for oxygen (Vind et al., 2018a, 2018b). Furthermore, it is believed that REEs may occur in other mineral phases formed during solidification of the slags (e.g., Al/Si-compounds) by atomic substitution. During the recovery of valuable metals by acid leaching of bauxite residue, silica gel can be formed due to the leaching of silicate minerals, which significantly affects the filtration efficiency of the leach liquor, i.e. reduced filterability. It is stated that under acidic conditions, below the isoelectric point for silica in the solution (i.e. pH_{iso} between 1.7 and 2.2) (Wilhelm and Kind, 2015), the hydrolysis of silica occurs very fast to produce silica monomers, H_4SiO_4 and $H_3SiO_4^-$ according to Reactions 1–3, which tend to form cyclic oligomers ($Si_{(n+1)}O_{(m+2)}OH$) via Ostwald ripening (Reaction 4) until a gel network is formed (Hamouda and Amiri, 2014; Tobler et al., 2009; Zerda et al., 1986).

$$M_2SiO_{4(s)} + 4HCl_{(l)} + H_2O_{(l)} \rightarrow 2MCl_{2(aq)} + H_2O_{(l)} + H_4SiO_{4(aq)} \quad (1)$$

$$M_2SiO_{4(s)} + 2H_2SO_{4(l)} + H_2O_{(l)} \rightarrow 2MSO_{4(aq)} + H_2O_{(l)} + H_4SiO_{4(aq)} \quad (2)$$

$$H_4SiO_{4(aq)} + H_2O_{(l)} \rightarrow H_3SiO_4^- + H_3O^+ \quad (3)$$

$$Si_nO_mOH + H_4SiO_{4(aq)} \rightarrow Si_{(n+1)}O_{(m+2)}OH + 2H_2O \quad (4)$$

It has been reported that during conventional acid leaching of bauxite residue at room temperature, a substantial decomposition of silicate compounds is achieved, which promotes the silicon dissolution and, consequently, the leach solution can no longer be filtered due to the polymerization of silica monomers (Rivera et al., 2017b, 2018). Due to the high concentration of silica in the slag, room-temperature acid leaching can no longer be considered because of silica polymerization. Hence, high-pressure acid leaching (or HPAL), i.e. acid leaching performed at high temperature in an autoclave, cannot only avoid problems associated to silica gel formation, but also to the depletion of other major metal such as titanium due to its hydrolysis at high temperature (Huang et al., 2015). Therefore, the acid consumption can be reduced and the extraction of REEs can be done selectively. This process has demonstrated promising results in the recovery of scandium from refractory lateritic nickel ore (Kaya and Topkaya, 2011, 2015), but also in the recovery of other valuable metals from nickel converter and smelter slags (Huang et al., 2015; Li et al., 2008).

In this work, the bauxite residue sample was mixed with different proportions of lignite coke, silica and lime, and smelted in an electric arc furnace for iron separation, so that different slags with low iron content were generated. The slags were cooled down at two different cooling rates. Subsequently, the leaching behaviour of selected rare earth elements (Sc, Y, La, Nd) by high-pressure acid leaching of the slag was analysed. Firstly, the REEs recovery by acid leaching of a slag with the highest content of aluminium, silicon and iron was studied. The acid concentration of two different mineral acids (HCl and H_2SO_4) and the leaching temperature were investigated. Secondly, the optimal conditions for REEs recovery from bauxite residue slags were established in terms of maximizing the extraction yield of REEs with the lowest dissolution of major elements (aluminium, iron, silicon, titanium). Thirdly, the untreated bauxite residue and the remaining slags (also generated by reductive smelting) were studied under optimal conditions to evaluate the effect of different chemical composition, mineralogy and morphology on the recovery of REEs. The treatment of bauxite residue and bauxite residue slags by HPAL was compared in terms of selected REEs, iron, aluminium and titanium concentration.

2. Material and methods

The bauxite residue used in this work was provided by Mytilineos S.A. - Aluminium of Greece (Agios Nikolaos, Greece). It was generated predominantly from Greek (karst) bauxite ore. Chemical analysis of the major elements (Al, Ti, Fe, Ca, Si, Na) was performed using wavelength-dispersive X-ray fluorescence spectroscopy (WDXRF, Panalytical PW2400). The concentration of selected rare earth elements (Sc, Y, La and Nd) were obtained by lithium metaborate ($LiBO_2$) fusion with nitric acid (3 vol% HNO_3) digestion followed by Inductively Coupled Plasma Mass Spectrometry (ICP-MS, Thermo Electron X Series) analysis.

The reductive smelting of bauxite residue was performed with three different mixtures of fluxes according to the distribution presented in Table 1. The corresponding amount of fluxes, i.e. CaO and SiO_2, were determined by FactSage 7.0 software (Bale et al., 2016) based on three different slag melting points. The major slag forming oxides (Al_2O_3, CaO, SiO_2 and TiO_2) were considered in the calculations. Na_2O was not considered in the calculations because of its low amount in the sample and its volatile behaviour during smelting. FeO_x was not used in the calculations as it is reduced to metallic iron during smelting. Each flux was prepared on the base of 1000 g of bauxite residue. The smelting reduction experiments were carried out in an electrical arc furnace (100 kVA direct current) at a temperature of 1500 ± 50 °C during 1 h. With each mixture of bauxite residue + flux + coke, three different slags were generated: slag I, II and III, respectively. After heating, the molten material was cooled down at two different cooling rates: (1) quenching with cold water (pouring the slag in water at room temperature, cooling rate about 1400 °C min^{-1}, fast cooling) and (2) room temperature cooling by keeping the slag in the crucible (cooling rate about 30 °C min^{-1}, slow cooling). Hence, the slag I

Table 1
Flux distribution, melting temperature and cooling rates for reductive smelting of bauxite residue.

Mixture	Bauxite residue, g	Flux, g			Melting temperature, °C	Cooling rate of slag[b]	Slag name[b]
		CaO	SiO_2	Lignite coke[a]			
I	1000	200	–	100	1350	Fast	Slag I.FC
I	1000	200	–	100	1350	Slow	Slag I.SC
II	1000	100	150	100	1390	Fast	Slag II.FC
II	1000	100	150	100	1390	Slow	Slag II.SC
III	1000	80	100	100	1485	Fast	Slag III.FC
III	1000	80	100	100	1485	Slow	Slag III.SC

[a] Lignite coke was composed by 87 wt% of carbon, 10 wt% ash content.
[b] Fast cooling (FC) = 1400 °C min^{-1}; Slow cooling (SC) = 30 °C min^{-1}.

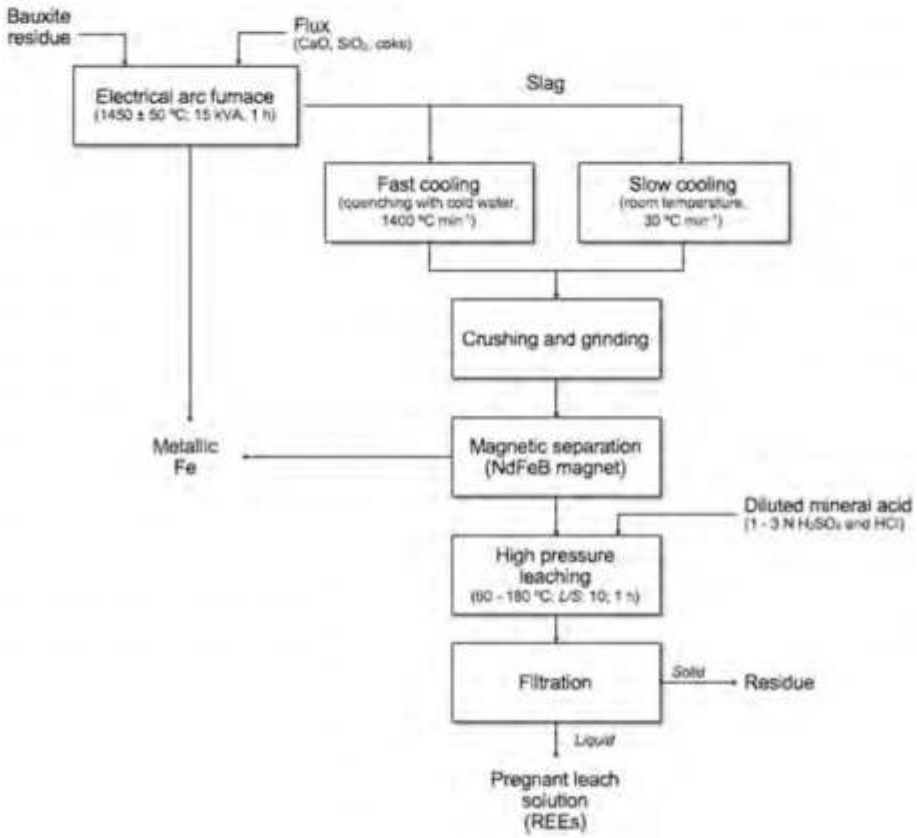

Fig. 1. Flow sheet for reductive smelting of bauxite residue, followed by high-pressure acid leaching of the slag arising during the smelting process.

subjected to fast and slow cooling are described as "slag I.FC" and "slag I.SC", respectively. The same denomination was considered for slags II and III. The iron metal fraction produced in the smelting experiment was separated from the slag and kept for further analysis. The slag was crushed into small pieces (< 2 cm) with a hammer and was subsequently crushed in a laboratory jaw crusher (Retsch BB 51) to produce material 100% finer than 1 mm. Later on, all the material was ground in a planetary ball mill (tungsten carbide grinding balls of 2 cm, 4 min at 510 rpm) to reduce the particle size to 100% < 400 μm (P_{80} = 135 ± 30 μm, P_{50} = 77 ± 22 μm). Small iron particles in the slag sample were removed by a NdFeB magnet after grinding. The magnet was covered with a plastic layer, and it was passed over the surface of the milled slag before sieving. These metallic pieces were subsequently removed and weighed. This procedure was repeated several times until no more magnetic particles were found attached to the magnet. The chemical analysis procedure for the slag is the same as the one described for the bauxite residue. Fig. 1 depicts the flow sheet for reductive smelting of bauxite residue, followed by high-pressure acid leaching of the slag arising during the smelting process.

High-pressure acid leaching experiments were carried out in a titanium autoclave (Parr Company, series 4560, 400 mL capacity) varying the temperature between 60 and 180 °C, in separate experiments, that led to an increase of the pressure by increasing the temperature. Consequently, the pressure increased from 0.3 bar at 60 °C until 15 bar at 180 °C when H_2SO_4 was used, while with HCl the pressure increased from 0.3 bar at 60 °C until 10 bar at 180 °C. The experiments were performed with a liquid-to-solid ratio, *L/S*, of 10:1 to ensure a substantial leaching concentration of REEs in the leach liquor with a reasonable consumption of bauxite residue. It must be noted that the utilization of low *L/S*-ratios does not enhance the recovery of REEs, with a concentration of less than 1 wt% in bauxite residue, due to the limited mass transfer as consequence of the high pulp density (Borra et al., 2015; Huang et al., 2015). Moreover, a ratio of 10:1 has been proposed as an optimal *L/S*-ratio for bauxite residue leaching (Alkan et al., 2018a). Analytical reagent grade H_2SO_4 (95–97 vol%, Sigma–Aldrich) and HCl (37 vol%, Fisher Scientific) were used in the present study as leaching reagents. The slurries after leaching were filtered using filter paper (pore size 0.45 μm) and diluted with 2 vol% HNO_3 (65 vol%, Chem-lab) for Inductively Coupled Plasma Optical Emission Spectroscopy (ICP-OES,

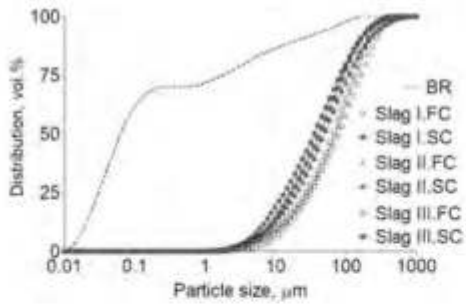

Fig. 2. Cumulative particle size distribution of the bauxite residue and the slags generated after melting (FC: fast cooling; SC: slow cooling; Slag I, II and III produced with mixture I, II and III, respectively).

Table 2
Major chemical components (in wt%) in the bauxite residue and in slag samples generated after smelting experiments.

Element	Bauxite residue	Slag I.FC	Slag I. SC	Slag II.FC	Slag II.SC	Slag III.FC	Slag III.SC
Al	9.6	20.2	20.0	16.9	17.8	19.3	19.1
Ca	6.1	27.2	27.1	17.7	15.9	16.9	16.3
Si	3.4	4.6	4.7	11.8	12.3	10.4	10.1
Ti	3.5	5.2	5.5	6.1	5.4	5.5	5.2
Na	2.1	1.8	0.9	2.2	2.0	2.1	2.3
Fe	32.7	1.5	2.5	2.0	2.4	2.5	3.7

FC: Fast cooling; SC: Slow cooling; Slag I, II and III produced with mixture I, II and III, respectively.

PerkinElmer Optima 8300) analysis of major (Al, Fe, Ti, Si) and minor elements (Sc, Y, La, Nd). The corresponding extraction yield of metal was calculated according to Eq. 5:

$$\% = \frac{Amount\ of\ metal\ in\ the\ leachate}{Total\ amount\ of\ metal\ in\ the\ sample} \quad (5)$$

The samples before and after leaching were embedded in epoxy resin and polished with SiC abrasive paper down to 1200 grit size followed by polishing with diamond paste (6, 3, and 1 μm) on a cloth disk. Then the samples were coated with platinum and analysed with a Scanning Electron Microscope (SEM-EDX, Philips XL30). The mineralogy of the samples before and after leaching was studied by X-ray powder diffraction (XRD, Bruker D2 Phaser). The obtained data were evaluated with EVA V.3.1 (Bruker AXS).

3. Results and discussion

3.1. Characterisation of the bauxite residue and slags

The cumulative particle size distributions of the bauxite residue and the slags samples produced after reductive smelting are shown in Fig. 2. In the bauxite residue, 90 vol% of the particles are smaller than 21 μm and 50 vol % of the particles are smaller than 0.06 μm. All the slags generated after smelting were crushed and milled at the same condition. Coarser particles were obtained with the slag subjected to fast cooling in comparison to the slag subjected to slow cooling. Thus, the slags subjected to fast cooling resulted in 90 vol% of the particles < 230 μm and 50 vol% of the particles < 75 μm. The slags subjected to slow cooling, on the other hand, resulted in 90 vol% of the particles < 180 μm and 50 vol% < 45 μm.

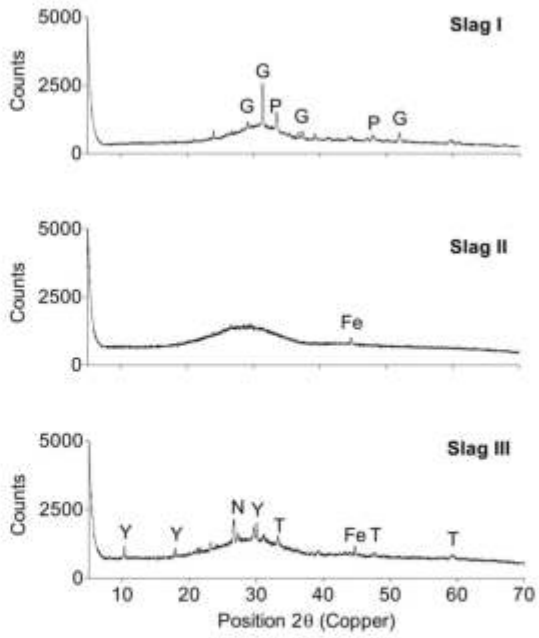

Fig. 3. XRD pattern of fast-cooled (FC) slags (G: gehlenite ($Al_2Ca_2SiO_7$); P: perovskite ($CaTiO_3$); Fe: metallic iron; Y: yoshiokaite ($Al_{5.4}Ca_{2.7}O_{16}Si_{2.7}$); N: nepheline ($AlNa_{0.98}O_4Si$); T: tricalcium aluminate ($Ca_3Al_2O_6$)).

The composition of major elements in the bauxite residue used in this study and in the slag generated after reductive smelting experiments is shown in Table 2. Iron is the main constituent in the bauxite residue sample (about 33 wt%). Iron was significantly removed during the smelting experiment, by which its concentration in the slag was low (< 4 wt%). The highest silicon concentration was obtained in slags II and III due to the addition of an excess of SiO_2 during smelting. The slag I resulted in the highest content of calcium due to the largest addition of CaO. In average, aluminium and titanium were enriched by a factor of 2 in the slag with respect to the original bauxite residue.

In Table 3, the concentrations of selected REEs (Sc, Y, La and Nd) are shown. The concentrations of all the REEs in the bauxite residue and the slags is shown in Table S1, in the Supplementary Material section. The concentration of these selected REEs were among the highest in the bauxite residue and in the slags. The concentration of REEs in the slags was increased by a factor of about 1.4 compared to the concentration of REEs in the bauxite residue sample.

Figs. 3 and 4 exhibit the XRD pattern of the slags generated after reductive smelting. It is stated that large cooling rates lead to high glass transition temperature (T_g), i.e. temperature range at which the molten material freezes into an amorphous solid without a discontinuity in the volume and the heat capacity and, consequently, allows the system a short period of time to relax. With low cooling rates, however, the molten material freezes at the melting temperature into a crystalline solid, with an abrupt discontinuity in both the volume and the heat capacity (Grest and

Table 3
Selected rare earth elements (in mg kg^{-1}) in the bauxite residue and in the slag samples generated after smelting experiments.

Element	Bauxite residue	Slag I.FC	Slag I. SC	Slag II.FC	Slag II.SC	Slag III.FC	Slag III.SC
Sc	97.8 ± 1.7	125.5 ± 2.0	122.5 ± 4.9	117.4 ± 1.4	128.3 ± 1.7	128.1 ± 1.5	124.0 ± 1.6
Y	65.7 ± 1.6	117.4 ± 1.1	118.2 ± 5.2	92.4 ± 0.7	105.2 ± 0.8	107.1 ± 1.6	105.6 ± 1.3
La	143.9 ± 3.0	211.9 ± 5.2	206.9 ± 18.0	159.2 ± 1.3	167.9 ± 2.7	174.8 ± 1.1	168.7 ± 1.5
Nd	64.8 ± 2.6	126.1 ± 2.1	126.9 ± 5.2	103.7 ± 1.0	111.2 ± 3.9	116.3 ± 2.2	111.8 ± 0.7

FC: Fast cooling; SC: Slow cooling; Slag I, II and III produced with mixture I, II and III, respectively.

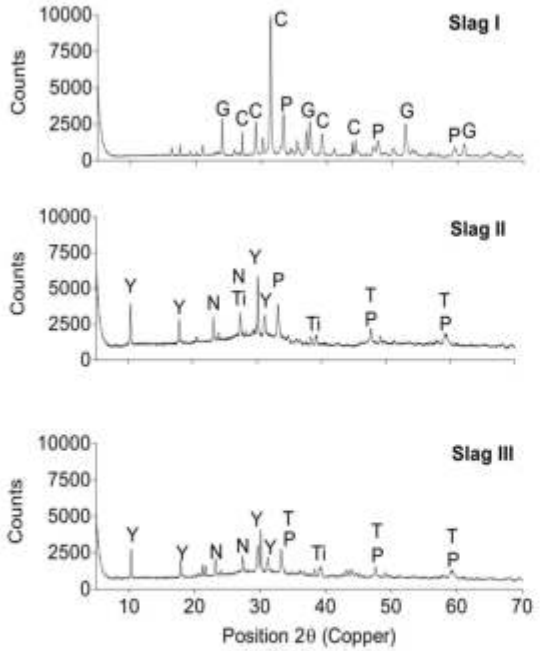

Fig. 4. XRD pattern of slow-cooled (SC) slags (G: gehlenite ($Al_2Ca_2SiO_7$); C: calcium magnesium silicate ($Ca_2MgO_7Si_2$); P: perovskite ($CaTiO_3$); Ti: calcium-silico-titanate (CaO_5SiTi); Y: yoshiokaite ($Ca_{7.5}Al_{15}SiO_{32}$); N: nepheline ($AlNa_{0.98}O_4Si$); T: tricalcium aluminate ($Ca_3Al_2O_6$)).

Cohen, 1980). The figures show that fast-cooled slags (Fig. 3) resulted in less crystalline mineral phases compared to the slags that were cooled down slowly at room temperature (Fig. 4). However, the particles of the slag subjected to fast cooling easily tend to agglomerate when the slags were ground in a planetary ball mill (Fig. 2) (Baláz, 2000; Van Loy et al., 2017). The same grinding conditions were applied to the other slags, but due to the crystallinity of the slags formed after slow cooling (Fig. 4), agglomeration did not occur, but only a particle size reduction was obtained (Fig. 2). Thus, from the slags that were cooled down slowly, slag I, which was produced with addition of 20 wt% CaO as flux, was mainly characterised by the presence of gehlenite and perovskite, although calcium magnesium silicate was also identified. Meanwhile, in slags II and III, similar mineralogical phases were recognized due to the use of CaO and SiO_2 as flux in slightly different proportions. Consequently, yoshiokaite, nepheline and tricalcium aluminate were the main mineral phases formed after cooling. The slag II subjected to fast cooling, however, resulted in an almost completely amorphous structure. The mineral phases identified in the slags differ significantly from the minerals and compounds identified in the original sample of bauxite residue: hematite and goethite (iron minerals); gibbsite and diaspore (aluminium minerals); calcite (calcium mineral); and cancrinite. SEM analysis on the smelted slag III.SC indicated that small particles of iron were locked in the slag phase, particularly in the Ca-Al-Si-Ti matrix phase (Fig. 5). These iron particles were not liberated from the slag matrix by grinding due to the very small size (< 50 μm).

In view of these results, slag III subjected to slow cooling, i.e. slag III.SC, represents the most unfavourable material to recover rare-earths by acid leaching, due to the high content of silicon, aluminium and iron. It must be noted that during conventional acid leaching, at room temperature, an over-saturation of silica in acid solution can lead to silica polymerization due to the hydrolysis of the silica monomers, i.e. H_4SiO_4 and $H_3SiO_4^-$, formed during the decomposition of silicate compounds (Hamouda and Amiri, 2014; Kokhanenko et al., 2016; Tobler et al., 2009). Silica gel formation represents a serious drawback in hydrometallurgy because the gel solutions can no longer be filtered (Abkhoshk et al., 2014; Alkan et al., 2018a; Queneau and Berthold, 1986; Shi et al., 2017; Zhang et al., 2016). Meanwhile, a high co-dissolution of aluminium and iron can significantly decrease the efficiency

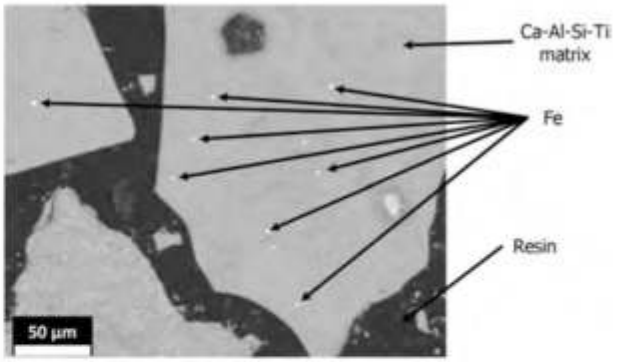

Fig. 5. SEM image of slag III.SC (10 kV, 200×, 10 WD).

of the further separation process, e.g., solvent extraction and/or ion exchange, to recover selectively the REEs due to their co-adsorption to the ion-exchange resins (Wang et al., 2011). Therefore, slag III.SC will be considered from now on as the main subject of this research. The remaining slags as well as bauxite residue were then studied afterwards under the experimental conditions that turned out to be the best for slag III.SC.

3.2. HPAL of a slag rich in silicon, aluminium and iron

The slag III.SC contained the highest content of silicon, aluminium and iron. This slag was leached with two different mineral acids (HCl and H_2SO_4) to evaluate the selectivity of the different elements. Leaching experiments were performed in the temperature range between 60 and 180 °C, and with acid concentrations of 1 and 3 N. The experiments were performed with a *L/S* ratio of 10 during 1 h.

3.2.1. HPAL with H_2SO_4

The effect of the temperature on the extraction of the major elements (Al, Fe, Ti and Si) with H_2SO_4 is shown in Fig. 6. As it has been reported in the literature, the dissolution of silicon in the leach solution increases with increasing acid concentration (Alkan et al., 2017; Rivera et al., 2018). Thus, the highest dissolution of silicon was about 80 wt%

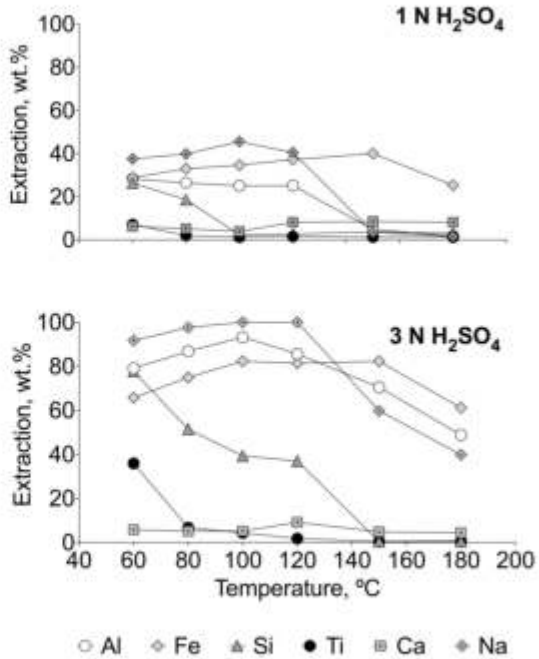

Fig. 6. Effect of the temperature and H_2SO_4 concentration on the dissolution of Al, Fe, Si, Ti, Ca and Na from slag III.SC (*L/S*: 10, t: 1 h).

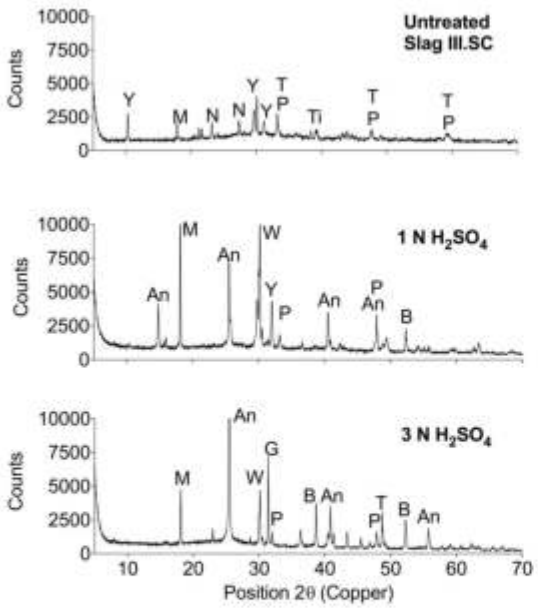

Fig. 7. XRD pattern of slag III.SC before and after HPAL with H_2SO_4 (sample at 150 °C) (Y: yoshiokate ($Al_{5.4}Ca_{2.7}O_{16}Si_{2.7}$); N: nepheline ($AlNa_{0.98}O_4Si$); T: tricalcium aluminate ($Ca_3Al_2O_6$); Ti: calcium-silico-titanate (CaO_5SiTi); An: anhydrite ($CaSO_4$); W: wollastonite ($CaSiO_3$); G: gehlenite ($Al_2Ca_2SiO_7$); P: perovskite (CaO_3Ti); M: mayenite ($Ca_{12}Al_{14}O_{33}$); B: bassanite ($CaSO_4 \cdot 0.5H_2O$)).

at 60 °C with 3 N H_2SO_4. Further increase in temperature led to a significant drop in silicon dissolution, particularly at temperatures above 130 °C (< 0.5 wt%), with the same acid concentration. This is because at high temperatures, water is released as vapour and, therefore, hydration of silica is substantially reduced. Hence, the partially hydrated metal ion reacts further with silicic acid, diminishing the condensation of monomeric silicic acid according to Reaction 6. The dehydrated silica precipitates and is readily filterable (Falayi et al., 2015; Huang et al., 2015; Whittington et al., 2003).

$$M_2SiO_{4(s)} + 2H_2SO_{4(l)} + (4n-2)H_2O_{(l)} \rightarrow 2MSO_4 \cdot nH_2O_{(l)} + SiO_{2(\text{filterable})} \quad (6)$$

As a result, the concentration of silicon in solution was < 0.5 g L^{-1} and no traces of silica gel formation was observed. The leaching process with low acid concentration resulted in a similar behaviour. It must be noted that < 1 wt% of silicon dissolution was obtained at 100 °C with 1 N H_2SO_4 (pH ~ 2.5). However, with 3 N H_2SO_4 (pH ~ 0.7), the same level of dissolution was observed just at 150 °C. This is because, with low acid concentration, the monomer's solubility is reduced as consequence of a fast reactivity of the acid with compounds of the solid particles. Moreover, high acid concentration and temperature enhance the decomposition of silicate compounds that lead to an increase of silicon dissolution (Colby et al., 1986; Wilhelm and Kind, 2015). High acid concentrations also led to high co-dissolution of aluminium and iron, which decrease the selectivity of the leaching process in terms of REEs recovery. Between 60 and 100 °C, about 80–95 wt% of aluminium was leached (ca. 18 g L^{-1}), while between 65 and 80 wt% of iron was transferred into the solution (ca. 3 g L^{-1}). A further increase in the leaching temperature, however, reduces the dissolution of aluminium, most probably caused by the lack of acid available for leaching due to the chemical precipitation of Ca^{2+} ions as $CaSO_4$ and the partial decomposition of silicate compounds. These phenomena have been reported earlier to occur in the presence of H_2SO_4, but not with HCl (Rivera et al., 2017a; Seidel and Zimmels, 1998). In addition, aluminium sulfate can also precipitate at high temperatures due to the evaporation of water (Sangita et al., 2017). The slight reduction of iron dissolution, in the range of temperature between 150 and 180 °C, can be explained by the formation of sodium-jarosite that was detected with low intensity only in the solid residue obtained after leaching at 180 °C. Sodium was totally dissolved when the leaching temperature was 100 °C, with a maximum concentration of 3 g L^{-1} in solution. A further increase in the leaching temperature caused sodium to precipitate, as its concentration at 180 °C was reduced till 0.9 g L^{-1} (about 40 wt%). The average iron concentration was 2.8 ± 0.3 g L^{-1}. The pH of the solution during leaching with 3 N H_2SO_4 was about 0.7 ± 0.1. Therefore, the precipitation of sodium and the acid conditions could explain the formation of jarosite at high temperatures (Duyvesteyn, 2012).

The extraction of titanium was < 5 wt%, particularly at high temperatures. This low dissolution of titanium has been attributed by different authors to the formation of $TiOSO_4$, which tends to have a low solubility (Alkan et al., 2018b; Borra et al., 2016d), but this phase was not detected during this investigation. However, the XRD analysis of the solid residue obtained after HPAL with H_2SO_4 (Fig. 7) confirmed that high acid concentration led to a large decomposition of silicate compounds, but also to the formation of $CaSO_4$. The formation of $CaSO_4$ can hinder the dissolution of titanium-containing mineral phases, such as perovskite ($CaTiO_3$) and/or calcium-silico-titanate (CaO_5SiTi), but also of Ca/Al/Si-compounds such as yoshiokaite ($Ca_{7.5}Al_{15}SiO_{32}$) and tricalcium aluminate ($Ca_3Al_2O_6$) (Fig. 4), as it was confirmed by SEM analysis. Fig. 8 describes the elemental distribution of the residue obtained after HPAL with H_2SO_4, while the quantitative analysis of elements is described in Table 4. The presence of a Ca-S-O phase (presumably $CaSO_4$) tends to enclose partially or totally the titanium-oxygen phase (TiO_2, presumably as anatase or rutile). The elemental mapping also confirmed the simultaneous occurrence of the Ca-S-O phase with silicon and aluminium, which could also explain the reduction of aluminium extraction at temperature above 100 °C. Although calcium-containing phases transform to their sulfate form easily, calcium dissolution is low due to the fact that calcium sulfates have very low solubility in water, i.e. 2 g L^{-1} at 20 °C (Myerson, 2002).

In Fig. 9, the effect of the temperature and acid concentration on the extraction of selected REEs (Sc, Y, La, Nd) after leaching with H_2SO_4 is shown. With low acid concentration, i.e. 1 N H_2SO_4, the extraction of scandium and yttrium was similar between 60 and 100 °C, i.e. 32 wt% (ca. 4 mg L^{-1}), but it was reduced when the temperature was increased up to 180 °C, presumably due to the co-precipitation with jarosite ($MFe_3(SO_4)_2(OH)_6$, where M can be Na^+, NH_4^+, H_3O^+, Li^+, K^+), as scandium can replace iron in its crystalline lattice structure (Duyvesteyn, 2012).

The extraction of lanthanum and neodymium was lower than 15 wt % over the whole temperature range. It must be noted that with 1 N H_2SO_4 the extraction of REEs is very low due to the high pH of the solution (~ 2.5) (Rivera et al., 2017a). Moreover, in acidic media, most of the REEs start dissolving only at pH values below 2, while the dissolution of major elements starts occurring at pH values below 5 (Borra et al., 2015). The highest extraction yield of REEs was obtained with 3 N H_2SO_4 between 60 and 100 °C. At temperatures higher than 100 °C, a gradual reduction of REEs recovery, with the exception of scandium, was observed. Several researches have reported a reduction of the lanthanides dissolution due to the formation of a sodium-lanthanide-double sulfate compound, i.e. $NaLn(SO_4)_2 \cdot nH_2O$, which has been observed in solid residues obtained after acid leaching of REEs-containing compounds (e.g., phosphogypsum, monazite and eudialyte minerals, pre-concentrated bastnasite mineral) with H_2SO_4 (Abreu and Morais, 2010; Davris et al., 2017; Kul et al., 2008; Meshram et al., 2016). Although sodium dissolution undergoes a substantial reduction at temperatures above 120 °C (Fig. 6), the sodium-lanthanide-double sulfate compound could not be detected by SEM-EDX none by XRD in our sample, probably due to the low concentration of the lanthanides and sodium (about 0.5 wt%). Therefore, it is believed that lanthanum and neodymium remain associated to the perovskite ($CaTiO_3$) phase, which was not totally dissolved after leaching, and is known to host REE (with Sc in very low concentration) in its matrix (Shrivastava et al., 2004;

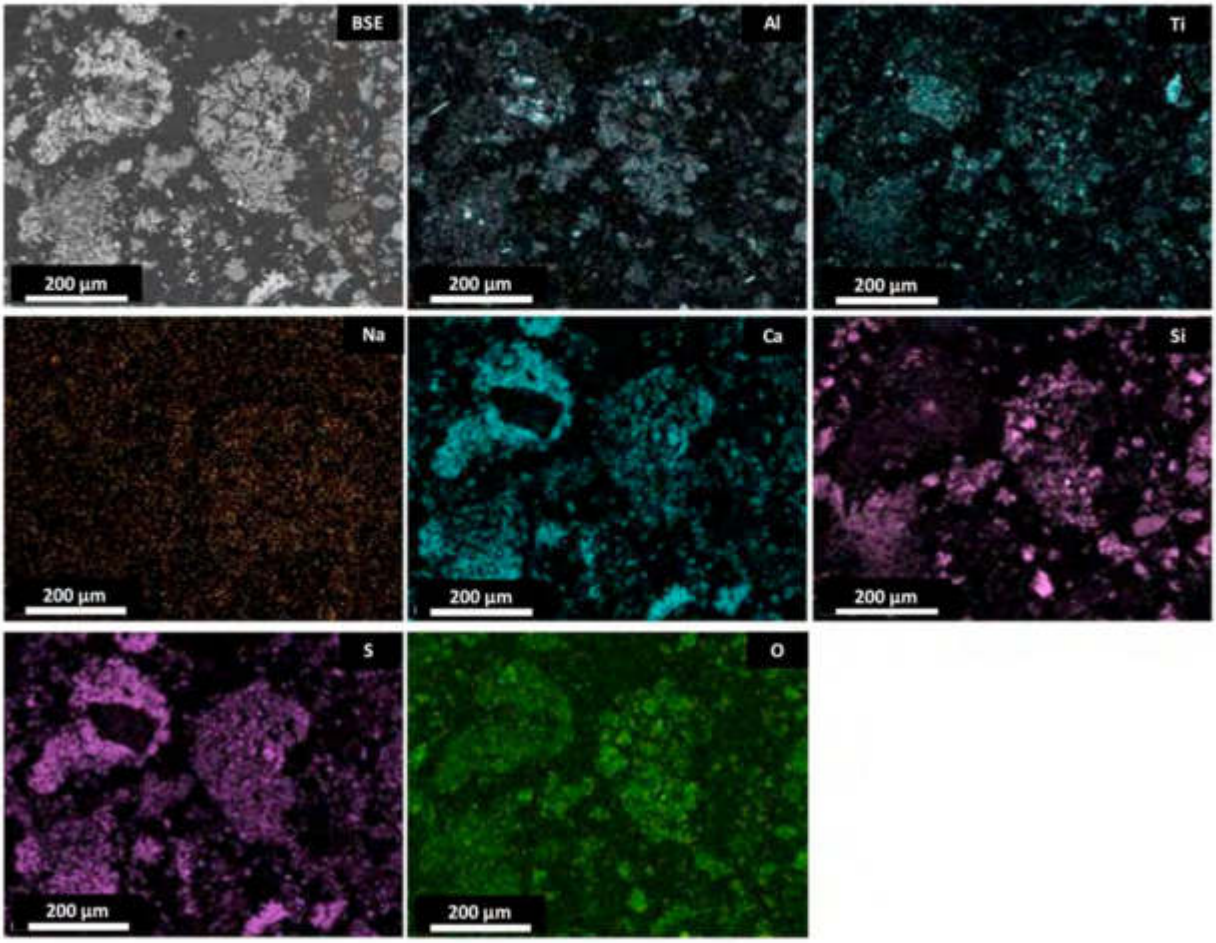

Fig. 8. Back-scattered electron (BSE) image of the leached slag III.SC with H_2SO_4 at 150 °C, and elemental distribution of Al, Ti, Na, Ca, Si, S and O.

Table 4
SEM-EDX (average) semi-quantitative analysis results of elements in Fig. 8.

Element	Concentration, wt%
Al	6 ± 5
Ti	5 ± 2
Na	0.5 ± 0.1
Ca	9 ± 8
Si	7 ± 5
S	7 ± 5
O	34 ± 6

Vind et al., 2018b; Zheng et al., 2016). The yttrium (and other heavy rare-earths) double sulfate is very soluble and, therefore, the decrease of yttrium extraction could be caused by the adsorption on silicon- and/or aluminium-oxide minerals, such as mayenite ($Ca_{12}Al_{14}O_{33}$), yoshiokaite ($Al_{5.4}Ca_{2.7}O_{16}Si_{2.7}$), tricalcium aluminate ($Ca_3Al_2O_6$) and/or gehlenite ($Al_2Ca_2SiO_7$), which were identified in the sample after leaching (Fig. 7). This phenomenon has been described earlier in the literature, and is supported by the observed similarity in extraction behaviour with increasing temperature between yttrium and aluminium, but also with silicon (Kosmulski, 1997). It is believed that due to the similar behaviour with yttrium, lanthanum and neodymium can also be adsorbed on the surface of the same mineral phases (Piasecki and Sverjensky, 2008). The reduction of scandium leaching at temperatures above 120 °C could be caused by the lack of acid produced by the chemical transformation of $CaCO_3$ into $CaSO_4$. The formation of jarosite could also explain the low recovery of scandium at high temperatures (Duyvesteyn, 2012).

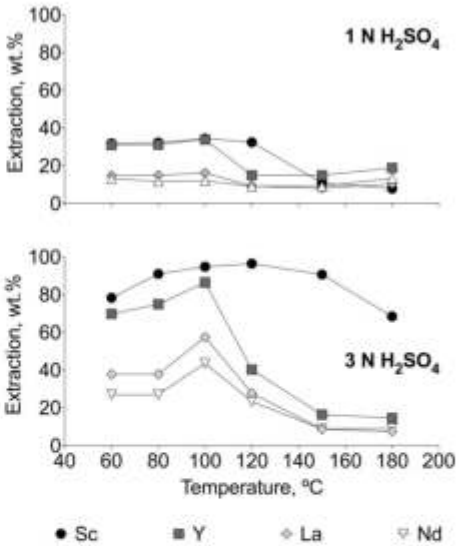

Fig. 9. Effect of the temperature and H_2SO_4 concentration on the extraction of selected REEs (Sc, Y, La, Nd) from the slag III.SC (*L/S*: 10, t: 1 h).

3.2.2. HPAL with HCl

Fig. 10 depicts the effect of the temperature and HCl concentration on the extraction of the major elements (Al, Fe, Ti and Si). High HCl concentration led to a significant dissolution of aluminium and iron, which is further enhanced by increasing the temperature. Silicon dissolution remained < 1 wt% due to the release of water as vapour at

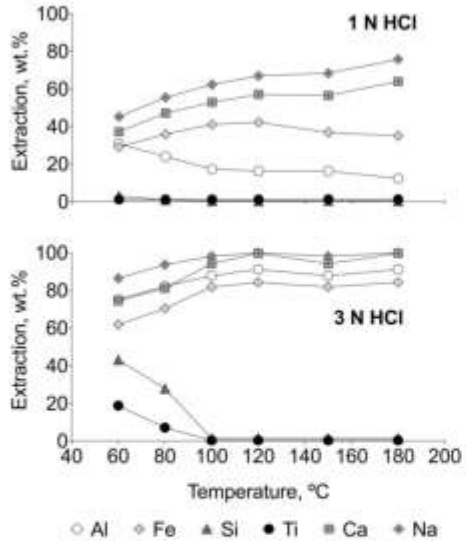

Fig. 10. Effect of the temperature and HCl concentration on the dissolution of Al, Fe, Si, Ti, Ca and Na from the slag III.SC (*L/S*: 10, t: 1 h).

high temperature, which inhibits the generation of silica gel (Reaction 7), similar to the case of HPAL with H_2SO_4.

$$M_2SiO_{4(s)} + 4HCl_{(l)} + (4n - 2)H_2O_{(l)} \rightarrow 2MCl_2 \cdot nH_2O_{(l)} + SiO_{2(\text{filterable})} \quad (7)$$

Table 5
SEM-EDX (average) semi-quantitative analysis results of elements in Fig. 11.

Element	Concentration, wt%
Al	5 ± 4
Ti	4 ± 6
Ca	2 ± 7
Na	1 ± 0.2
Si	8 ± 3
O	31 ± 8

Fig. 11 describes the elemental distribution of the residue obtained after HPAL with HCl, while the quantitative analysis based on the elemental mapping by SEM-EDX is shown in Table 5. As it was observed before in the residue obtained after leaching with H_2SO_4 (Fig. 8), titanium was also found simultaneously with silicon and aluminium in the residue obtained after leaching with HCl. The low extraction of titanium could be caused by its chemical association to the perovskite phase, which in this case was not totally decomposed after HPAL with HCl (see Fig. 12).

The effect of the temperature and the HCl concentration on the extraction of scandium, yttrium, lanthanum and neodymium is shown in Fig. 13. With 1 N HCl, the extraction yield of yttrium, lanthanum and neodymium significantly increased when the temperature was increased. Neodymium and lanthanum showed a comparable leaching behaviour, as they occur only in the +III valence state and tend to have a similar mineralogical distribution in bauxite residue (Lei et al., 1986;

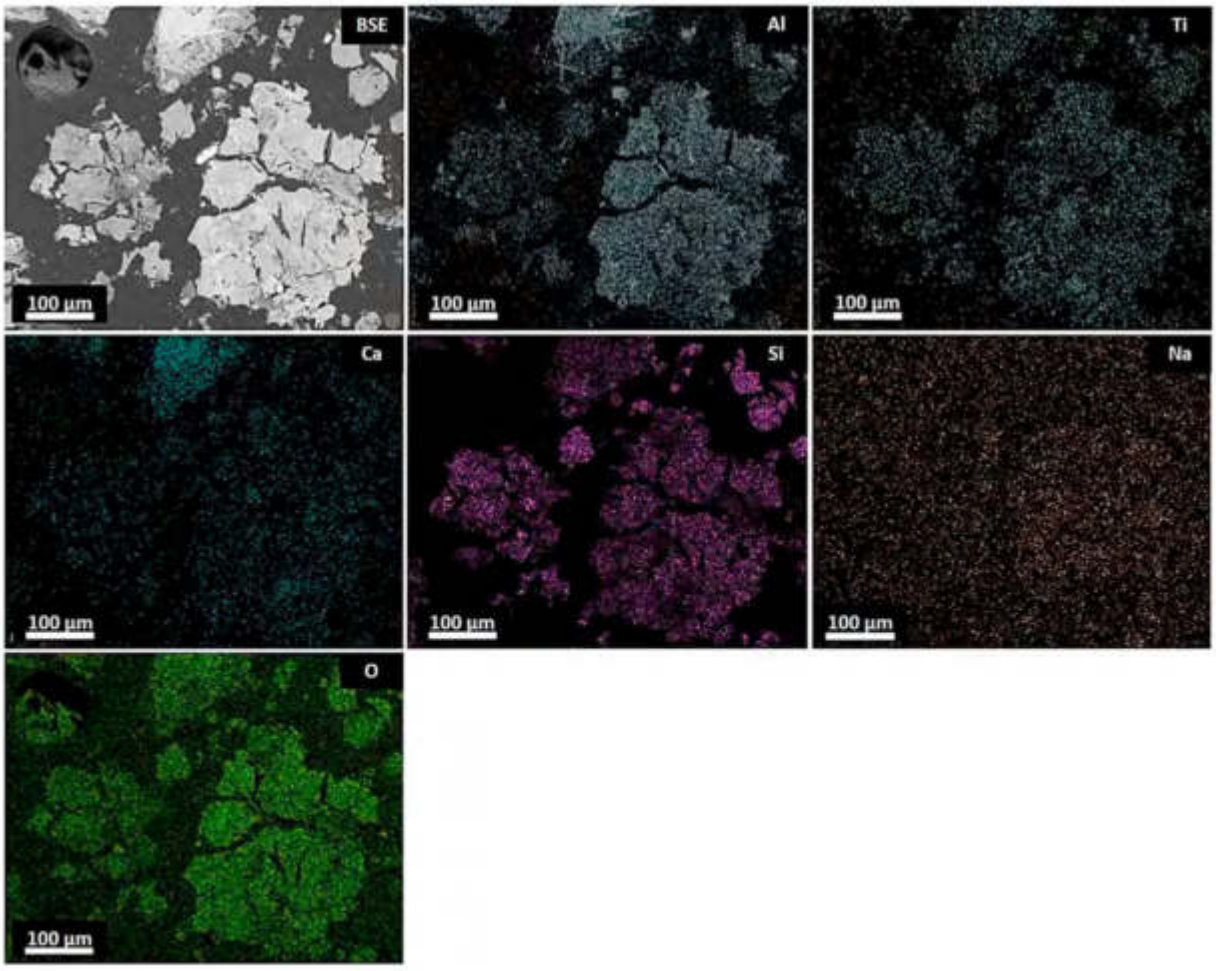

Fig. 11. Back-scattered electron (BSE) image of the leached slag III.SC with HCl at 120 °C, and elemental distribution of Al, Ti, Ca, Si and O.

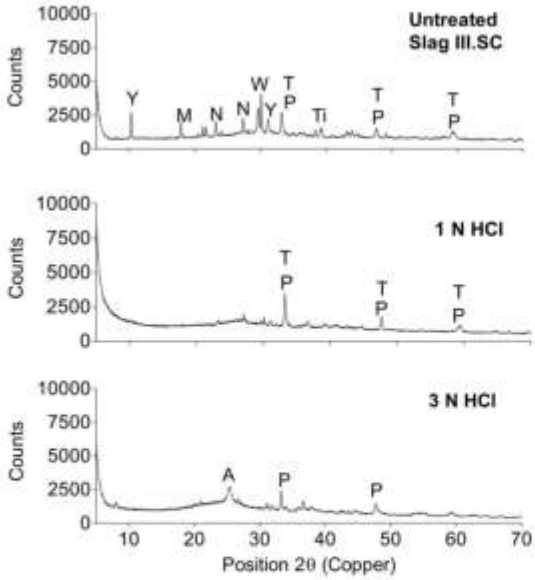

Fig. 12. XRD pattern of slag III.SC before and after HPAL with HCl (sample at 120 °C) (Y: yoshiokaite ($Al_{5.4}Ca_{2.7}O_{16}Si_{2.7}$); N: nepheline ($AlNa_{0.98}O_4Si$); T: tricalcium aluminate ($Ca_3Al_2O_6$); Ti: calcium-silico-titanate (CaO_5SiTi); W: wollastonite ($CaSiO_3$); P: perovskite (CaO_3Ti); A: anatase (TiO_2); M: mayenite ($Ca_{12}Al_{14}O_{33}$)).

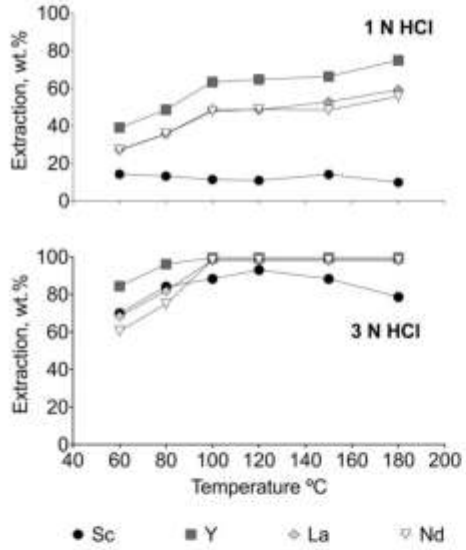

Fig. 13. Effect of the temperature and HCl concentration on the extraction of selected REEs (Sc, Y, La, Nd) from the slag III.SC (*L/S*: 10, t: 1 h).

Rivera et al., 2018). However, scandium was scarcely leached out from the solid matrix with low HCl concentration, due to its association to the tricalcium aluminate ($Ca_3Al_2O_6$) mineral phase. According to the XRD analysis shown in Fig. 12, $Ca_3Al_2O_6$ was detected in similar scanned angles as that of the perovskite (CaO_3Ti) phase, not only in the unprocessed slag sample, but also in the solid residue obtained after leaching with 1 N HCl. However, among the REEs, the scandium concentration in the perovskite phase can be almost negligible (Vind et al., 2018a). Previous reports have shown that it remains associated to aluminium compounds (Borra et al., 2016b, 2017). $Ca_3Al_2O_6$ was not detected in the solid residue obtained after leaching with 3 N HCl, presumably due to its total decomposition, which may explain the high REEs recovery at temperatures > 100 °C. The decrease of scandium recovery above 120 °C could be caused by its adsorption on silica, which started to precipitate at temperatures above 100 °C (Fig. 10).

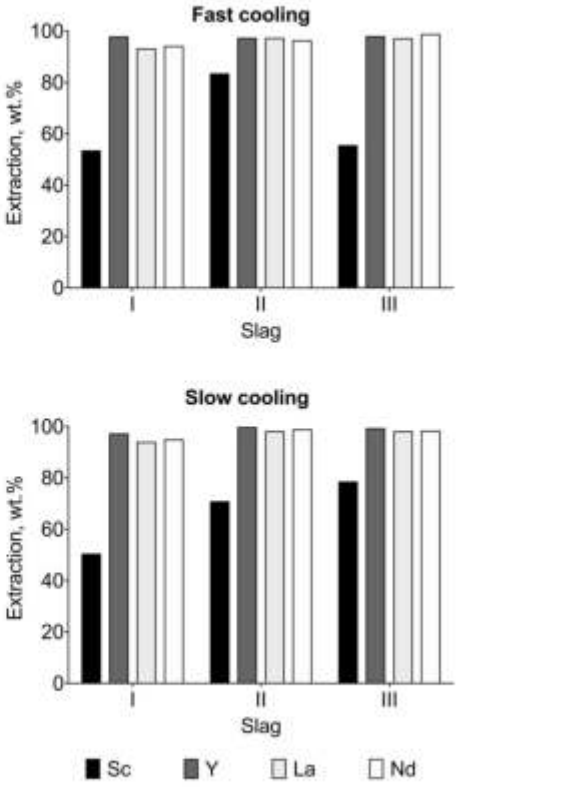

Fig. 14. Extraction of selected REEs (Sc, Y, La and Nd) after HPAL with HCl of fast and slow cooled slag from bauxite residue by reductive smelting (acid concentration: 3 N, 120 °C, *L/S*: 10, *t*: 1 h).

This phenomenon has been reported in the literature and could be confirmed by these results (Ma et al., 2014).

3.3. REEs recovery by HPAL from other slags of bauxite residue smelting

Other slags than III.SC, presented in Tables 2 and 3, were processed by HPAL under the conditions that were optimized for slag III.SC (see section 3.2). To recapitulate, the highest extraction yield of REEs was obtained with an acid concentration of 3 N, with both acids: HCl and H_2SO_4. The optimal temperature was defined in terms of the lowest concentration of aluminium, iron, titanium and silicon in the solution, in order to enhance the selectivity for REEs recovery. Thus, in the case of HPAL with HCl, the lowest aluminium/iron (Al/Fe) and scandium/iron (Sc/Fe) leaching ratios (i.e. 1.1 and 0.9, respectively) were obtained at 120 °C with a high REEs extraction (Sc: 79 wt%; Y, Nd and La > 97 wt%) and very low concentration of titanium and silicon in the solution (< 0.5 g L^{-1}). In the case of HPAL with H_2SO_4, the lowest Al/Fe and Sc/Fe (i.e. 0.9 and 1.1) ratios were obtained at 150 °C, at which the Sc/ΣREEs ratio was the highest one (i.e. 3) and, therefore, at high selectivity for scandium recovery (ΣREEs was considered as the sum of yttrium, lanthanum and neodymium extraction).

The extraction of selected REEs (Sc, Y, La, Nd) from the remaining slags by HPAL, with HCl and H_2SO_4, are summarized in Figs. 14 and 16, respectively. Similar to the behaviour of slag III.SC, HPAL with HCl showed a high recovery of REEs. Meanwhile, with H_2SO_4, scandium was preferentially dissolved over the other REEs, presumably due to the formation of a $CaSO_4$ product layer on the surface of the solid particles (see section 3.2.1, Fig. 8). The solid residue obtained after leaching with H_2SO_4 was highly crystalline due to the formation of $CaSO_4$ (Fig. 17). The solid residue after leaching with HCl, on the contrary, resulted in a quite amorphous structure, and unveiled the presence of titanium-rich phases, which were formed even with a fast cooling rate. It must be noted that Borra et al. were able to suppress the $CaTiO_3$ formation by

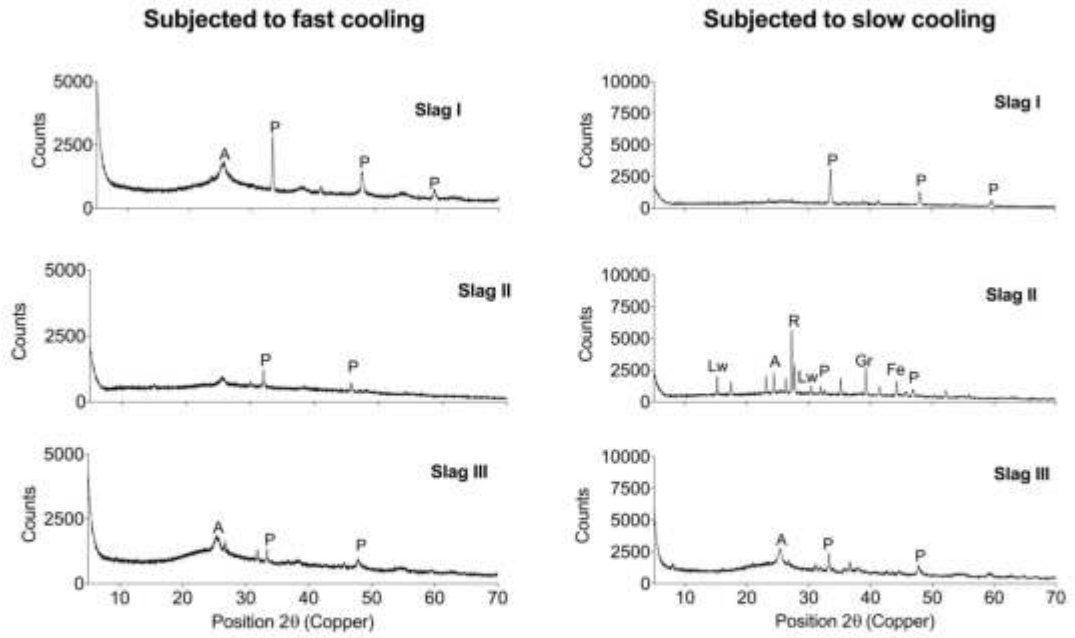

Fig. 15. XRD pattern of different slags treated by HPAL with 3 N HCl at 120 °C (*L/S*: 10, *t*: 1 h; A: anatase (TiO_2); P: perovskite ($CaTiO_3$); Fe: metallic iron; Lw: lawrencite ($FeCl_2$); R: rutile (TiO_2); Gr: grossite (Al_4CaO_7)).

quenching the slag produced during smelting of a solid residue with very low aluminium content (< 1 wt%), which was generated by alkali roasting followed by water leaching. In this investigation, the use of a pre-treatment process prior to reductive-smelting was not considered. According to Fig. 15, titanium-rich phases (i.e. perovskite, anatase, rutile) are less soluble in HCl-media, as their peaks were the most evident in the corresponding diffractograms of XRD analysis. The highest recovery of scandium (ca. 85 wt%) was obtained from slag II subjected to a fast cooling (slag II.FS in Tables 2 and 3), which was the most amorphous one among all the other slags (Fig. 3) and, therefore, the easiest one to leach. Therefore, the treatment of this slag by HPAL can be further optimized by reducing the leaching temperature and/or the acid concentration. The figures also show that, from slag I (formed by the mere use of CaO as flux during smelting of bauxite residue) up to 60 wt% of scandium was recovered, presumably due the formation of $CaSO_4$ during leaching, but also due to the presence of grossite (aluminium rich) and laihuinite (iron rich) compounds (Fig. 17), as scandium can be part of their corresponding lattice matrix. On the other hand, scandium was mostly extracted from slags II and III, particularly the ones subjected to slow cooling rates, which were characterised by the presence of yoshiokaite and nepheline (both aluminium-silicate compounds), and leached with H_2SO_4. This can be explained by the preferential decomposition of such compounds in H_2SO_4 rather than with HCl (Rivera et al., 2018). In slag I, however, aluminium was found together with calcium in the mineral phase gehlenite, but not associated with silicon, which can also explain the low scandium recovery from this slag. Therefore, it is believed that aluminium-calcium compounds may have a lower solubility in acidic media compared to aluminium-silicate compounds, which may limit the recovery of scandium and other REEs from the slags.

3.4. Direct treatment of bauxite residue by HPAL versus HPAL of bauxite residue slags and other acid leaching processes

The direct treatment of Greek bauxite residue by HPAL was performed with HCl and H_2SO_4 in order, according to the diagram presented in Fig. 18, to evaluate the recovery of REEs in the presence of a high content of iron (33 wt%, Table 2). HPAL with H_2SO_4 (Fig. 19) allows a relatively high recovery of REEs up to 100 °C, without bringing too much iron into the solution (< 10 wt%), but with a substantial co-dissolution of silicon (ca. 60 wt%). A further increase of the temperature led to ca. 70 wt% of scandium recovery, presumably due to the decomposition of the iron-rich mineral phases, e.g., hematite, goethite, which are the main host minerals for scandium in this particular bauxite residue (Vind et al., 2018a). Nevertheless, the recovery of other REEs was relatively low (< 45 wt%) due to the high dissolution of sodium (> 40 wt%) that may lead to the formation of double sulfates

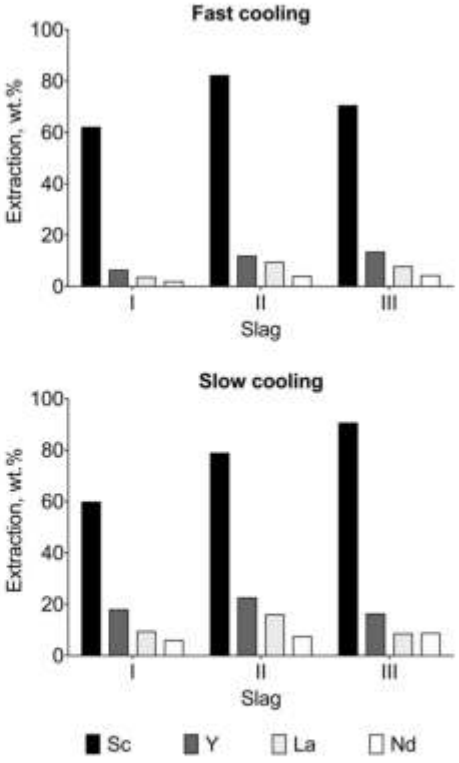

Fig. 16. Extraction of major Al, Fe and selected REEs (Sc,Y, La and Nd) after HPAL with H_2SO_4 of fast and slow cooled slags from bauxite residue by reductive smelting (acid concentration: 3 N, 150 °C, *L/S*: 10, *t*: 1 h).

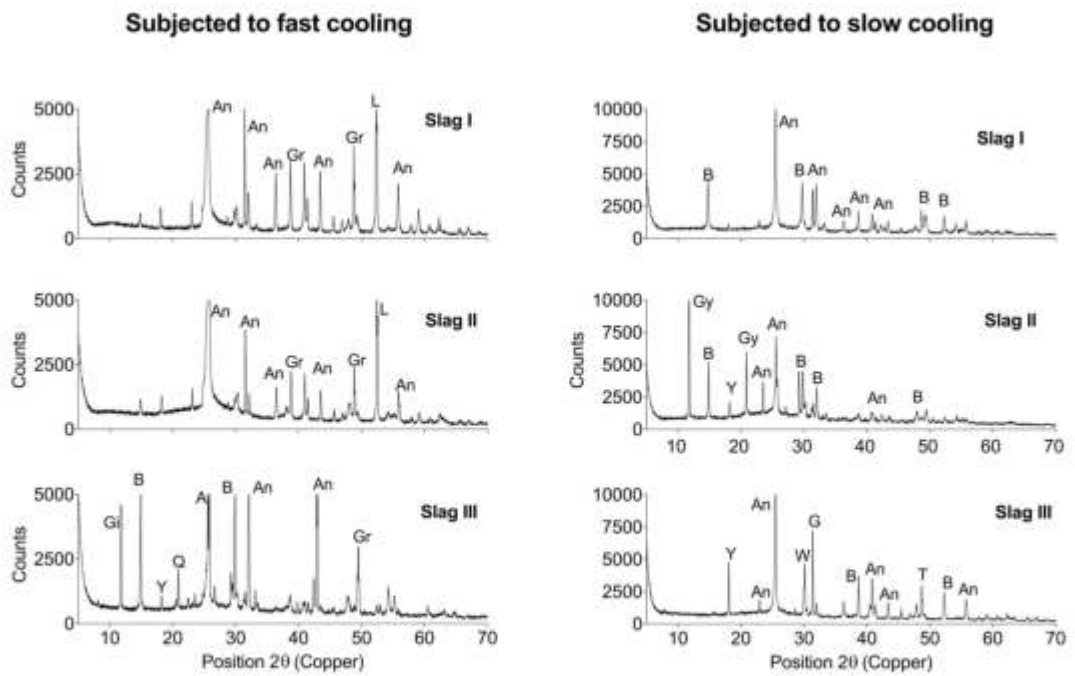

Fig. 17. XRD pattern of different slags treated by HPAL with 3 N H_2SO_4 at 150 °C (*L/S*: 10, *t*: 1 h; An: anhydrite ($CaSO_4$); Gr: grossite (Al_4CaO_7); L: laihuinite ($Fe^{2+}Fe^{3+}{}_2(SiO_4)_2$); Gi: gismondine ($Ca_2Al_4Si_4O_{16}{\cdot}9(H_2O)$; Q: quartz ($SiO_2$); B: bassanite ($CaSO_4{\cdot}0.5H_2O$); A: anatase ($TiO_2$); T: tricalcium aluminate ($Ca_3Al_2O_6$); G: gehlenite ($Al_2Ca_2SiO_7$); M: mayenite ($Ca_{12}Al_{14}O_{33}$); Gy: gypsum ($CaSO_4{\cdot}2H_2O$); Y: yoshiokaite ($Ca_{7.5}Al_{15}SiO_{32}$)).

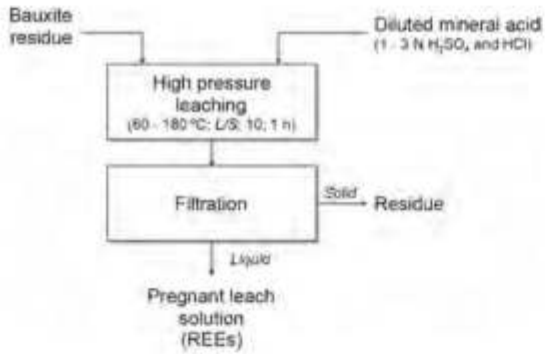

Fig. 18. Flow sheet for high-pressure acid leaching of the bauxite residue sample.

(Abreu and Morais, 2010; Davris et al., 2017; Kul et al., 2008; Meshram et al., 2016). HPAL with HCl (Fig. 20) allowed the precipitation of silicon and titanium at temperatures above 100 °C, beside high recoveries for scandium (> 70 wt%) and other REEs (La: 67–80 wt%, Nd and Y > 88 wt%). The substantial co-dissolution of iron and aluminium, however, was unavoidable at high temperatures and acidic conditions. Nevertheless, HPAL of (untreated) bauxite residue should still be investigated in detail. The optimization of the leaching parameters (e.g., leaching time, *L/S*-ratio and leaching temperature) affecting the extraction of REEs from different slags, produced during the smelting process of bauxite residue, can be further investigated by, for example, using the Taguchi method (Bayca and Kisik, 2018).

It must be noted that the extraction yields obtained at temperatures < 100 °C are comparable to the ones reported by other researchers, who have also investigated the direct treatment of bauxite

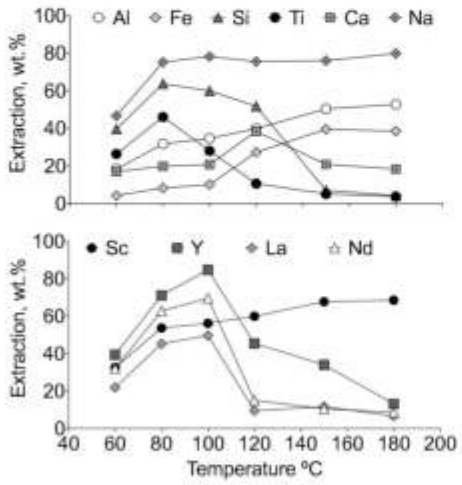

Fig. 19. High-pressure acid leaching of bauxite residue with 3 N H_2SO_4 at different temperatures (*L/S*: 10, t: 1 h).

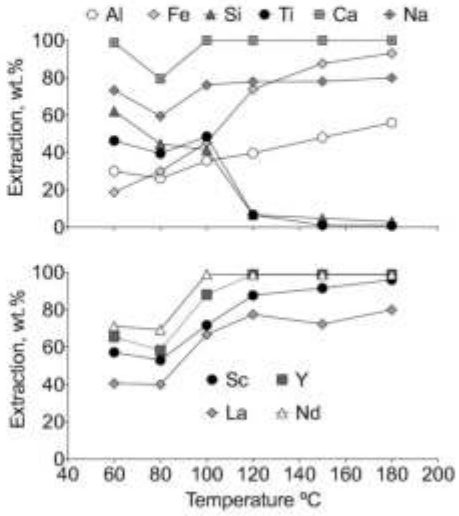

Fig. 20. High-pressure acid leaching of bauxite residue with 3 N HCl at different temperatures (*L/S*: 10, t: 1 h).

residue by acid leaching. Thus, Borra et al. have reported REE recoveries in the range of 70–80 wt%, by treating the bauxite residue via direct acid leaching with *L/S*-ratio of 50:1, in order to enhance the extractability of REEs. Up to 50 wt% of scandium can be recovered with < 5 wt% of iron in the solution, while aluminium, silicon and titanium are significantly dissolved (Borra et al., 2015). In another study, the use of strong oxidative conditions (e.g., addition of H_2O_2) to avoid silica polymerization has also been reported (Alkan et al., 2018a). According to the authors, by treating the bauxite residue at 90 °C, with an equal concentration of 2.5 M of H_2O_2 and H_2SO_4 directly, an extraction of approximately 70 wt% of scandium can be achieved with a substantial depletion of silica dissolution, but about 35 wt% of iron is also extracted in the process. The method, however, allows the recovery of about 90 wt% of titanium as $[TiO\text{-}O]SO_4$ complex. The mixture of bauxite residue with concentrated mineral acids, at very high solid-liquid ratio, followed by water leaching, has also been studied as a process to avoid silica polymerization (Rivera et al., 2018). The application of this method has demonstrated a recovery up to 40 wt% of scandium (and up to 50 wt% of other REEs) with a significant co-dissolution of iron (about 25 wt%), but the concentration of REEs in the leachate can be enhanced by considering a multi-stage leaching with the recirculation of the leach liquor (Rivera et al., 2018).

As described in the previous section, during the treatment of slags from bauxite residue smelting by HPAL, silicon remains undissolved in the solid residue and, consequently, silica polymerization is avoided. Titanium also remains in the solid residue, but its recovery after leaching would be beneficial. Furthermore, HPAL of the slags allows to recover > 90 wt% of scandium without bringing too much iron into the solution ($< 3\,g\,L^{-1}$). The recovery of other REEs is high when using HCl. However, the large volume of effluents enriched with HCl may represent the major concern in the process due to its high corrosiveness. The use of glass-lined reactors and valves and pipes made with high-performance chemically-resistance polymers can significantly increase the capital cost. From this point of view, the recovery of scandium from the slags can alternatively be done by using H_2SO_4, which is widely used in the industry and allows a high extraction yield, although the recovery of other REEs is low. The residues generated after HPAL are rich in silica and low in sodium content. They can also be rich in $CaSO_4$ when H_2SO_4 is considered in the process. The residue can be further studied for their applicability in building materials or cementitious binder.

4. Conclusions

Iron was successfully separated from Greek bauxite residue by using different mixtures of coke, CaO and SiO_2 at a temperature of 1500 °C. After heating, the slag solidified slowly at room temperature resulted in a more crystalline phases than the slag subjected to quenching (fast cooling). The slag III, subjected to slow cooling, was used as a reference to selectively recover rare-earths by HPAL due to its high content of silicon, aluminium and iron. HPAL of slags produced during the smelting of bauxite residue effectively suppressed the co-dissolution of silicon and titanium, particular at temperatures above 100–120 °C. HPAL with HCl allows an extraction up to 90 wt% of scandium, and about 95 wt% of yttrium, lanthanum and neodymium at temperatures above 100 °C. However, by performing HPAL with H_2SO_4, the extraction of scandium reached up to 95 wt% at 150 °C, while the extraction yield of yttrium, lanthanum and neodymium was about 40 wt%. The formation of $CaSO_4$ during HPAL with H_2SO_4 hinders the dissolution of TiO_2, but also the dissolution of other REEs, with less effect on scandium extraction. Meanwhile, the extraction of lanthanum and neodymium is presumably limited by their chemical association to the perovskite phase and/or by their adsorption on the surface of silicon/aluminium-oxide minerals, which could be confirmed with microscopy analytical techniques such as transmission electron microscopy and electron probe micro analysis. Nevertheless, the formation of sulfates result in an increase in the selectivity of scandium over the other REEs. The optimal conditions determined from the reference slag were successfully applied to other slags from bauxite residue smelting. HPAL with HCl at 120 °C allowed to obtain high extraction yields for yttrium, lanthanum and neodymium (> 90 wt%), but the slag II subjected to fast cooling (amorphous slag) resulted in the highest extraction yield of scandium (about 85 wt%). The treatment of slag I and III, both subjected to slow cooling, with H_2SO_4 at 150 °C, resulted also in a substantial scandium dissolution (about 90 wt%), but with very low dissolution of other REEs. About 70 wt% of scandium can be recovered from the (untreated) bauxite residue by HPAL together with a high co-dissolution of other major elements (aluminium, iron, titanium and silicon). Although the treatment of slag from bauxite residue by HPAL has demonstrated better performance in terms of REEs recovery than other reported technologies, the process still requires further investigation to optimize the acid consumption, leaching time, *L/S*-ratio and leaching temperature. An economic analysis should be developed in order to assess the economic feasibility for bauxite residue and bauxite residue slag processing via HPAL.

Acknowledgements

The research leading to these results has received funding from the European Community's Horizon 2020 Programme (H2020/2014–2019) under Grant Agreement No. 636876 (MSCA- ETN REDMUD). This publication reflects only the authors' view, exempting the Community from any liability. Project website: http://www.etn.redmud.org. The authors thank Aluminium of Greece for providing the bauxite residue sample.

Appendix A. Supplementary data

Supplementary data to this article can be found online at https://doi.org/10.1016/j.hydromet.2019.01.005.

References

Abkhoshk, E., Jorjani, E., Al-Harahsheh, M.S., Rashchi, F., Naazeri, M., 2014. Review of the hydrometallurgical processing of non-sulfide zinc ores. Hydrometallurgy 149, 153–167. https://doi.org/10.1016/j.hydromet.2014.08.001.

Abreu, R.D., Morais, C.A., 2010. Purification of rare earth elements from monazite sulphuric acid leach liquor and the production of high-purity ceric oxide. Miner. Eng. 23, 536–540. https://doi.org/10.1016/j.mineng.2010.03.010.

Alkan, G., Xakalashe, B., Yagmurlu, B., Kaussen, F., Friedrich, B., 2017. Conditioning of red mud for subsequent titanium and scandium recovery – a conceptual design study. World Metall. – Erzmetall 70, 5–12.

Alkan, G., Yagmurlu, B., Cakmakoglu, S., Hertel, T., Kaya, Ş., Gronen, L., Stopic, S., Friedrich, B., 2018a. Novel approach for enhanced scandium and titanium leaching efficiency from bauxite residue with suppressed silica gel formation. Sci. Rep. 8, 5676. https://doi.org/10.1038/s41598-018-24077-9.

Alkan, G., Yagmurlu, B., Xakalashe, B., Stopic, S., Friedrich, B., 2018b. Enhancement of Sc and Ti extraction rates from Fe-depleted slag by hydrogen peroxide and sulfuric acid leaching. In: Pontikes, Y. (Ed.), 2nd International Bauxite Residue Valorisation and Best Practices Conference, pp. 255–261 Athens.

Baláz, P., 2000. Extractive Metallurgy of Activated Minerals, 10th ed. Amsterdam.

Bale, C.W., Bélisle, E., Chartrand, P., Decterov, S.A., Eriksson, G., Gheribi, A.E., Hack, K., Jung, I.H., Kang, Y.B., Melançon, J., Pelton, A.D., Petersen, S., Robelin, C., Sangster, J., Spencer, P., Van Ende, M.A., 2016. Reprint of: FactSage thermochemical software and databases, 2010–2016. Calphad 54, 35–53. https://doi.org/10.1016/j.calphad.2016.07.004.

Bayca, S.U., Kisik, H., 2018. Optimization of leaching parameters of aluminum hydroxide extraction from bauxite waste using the taguchi method. Environ. Prog. Sustain. Energy 37, 196–202. https://doi.org/10.1002/ep.12654.

Binnemans, K., Jones, P.T., Blanpain, B., Van Gerven, T., Pontikes, Y., 2015. Towards zero-waste valorisation of rare-earth-containing industrial process residues: a critical review. J. Clean. Prod. 99, 17–38. https://doi.org/10.1016/j.jclepro.2015.02.089.

Borra, C.R., Pontikes, Y., Binnemans, K., Van Gerven, T., 2015. Leaching of rare earths from bauxite residue (red mud). Miner. Eng. 76, 20–27. https://doi.org/10.1016/j.mineng.2015.01.005.

Borra, C.R., Blanpain, B., Pontikes, Y., Binnemans, K., Van Gerven, T., 2016a. Recovery of rare earths and other valuable metals from bauxite residue (red mud): a review. J. Sustain. Met. 2, 365–386. https://doi.org/10.1007/s40831-016-0068-2.

Borra, C.R., Blanpain, B., Pontikes, Y., Binnemans, K., Van Gerven, T., 2016b. Smelting of bauxite residue (red mud) in view of iron and selective rare earths recovery. J. Sustain. Metall. 2, 28–37. https://doi.org/10.1007/s40831-015-0026-4.

Borra, C.R., Blanpain, B., Pontikes, Y., Binnemans, K., Gerven, Van, om, T., 2016c.